Composites: Part B 69 (2015) 592–602

Contents lists available at ScienceDirect

Composites: Part B

journal homepage: www.elsevier.com/locate/compositesb

Three dimensional elasticity solution for static and dynamic analysis of multi-directional functionally graded thick sector plates with general boundary conditions

Hassan Zafarmand, Mehran Kadkhodayan *

Department of Mechanical Engineering, Ferdowsi University of Mashhad, Mashhad 91775-1111, Iran

ARTICLE INFO

Article history:
Received 11 April 2014
Received in revised form 10 October 2014
Accepted 29 October 2014
Available online 7 November 2014

Keywords:
A. Plates
C. Finite Element Analysis
B. Elasticity
B. Impact behaviour

ABSTRACT

In this study, the three dimensional static and dynamic behavior of a thick sector plate made of two-directional functionally graded materials (2D-FGMs) is investigated. Material properties are assumed to be graded in both radial and thickness directions according to a simple power law distribution in terms of the volume fractions of the constituents. The governing equations are based on the 3D theory of elasticity. Employing 3D graded finite element method (GFEM) based on the Hamilton's principle and Rayleigh–Ritz energy method, the equations are solved in space and time domains. In the case of static analysis, the sector plate is subjected to a uniform pressure load and for dynamic analysis is subjected to an impact loading. The effects of material gradient index, boundary condition and thickness to radius ratio of the sector plate on the static and dynamic responses are presented and discussed.

1. Introduction

In recent years, in order to optimize the responses of structures subjected to thermal and mechanical loads, a new category of composite materials known as functionally graded materials (FGMs) is often used in structural components. An FGM is a composite material, microscopically inhomogeneous and fabricated from two or more constituent phases with a defined composition, in which the mechanical properties vary smoothly and continuously from one surface to the other [1]. This idea which was used for the first time by Japanese researchers [2], leads to the concept of FGMs.

The mechanical behavior of FGMs with various geometries and loading conditions has been studied by many researchers. Among these geometries, the sector plates are of practical concern in many fields of engineering, such as mechanical and civil with many industrial applications including curved bridge decks, building floor slabs, steam turbine diaphragms.

It should be noted that the plate is a three dimensional (3D) structure that one dimension is much smaller than the other dimensions. In 2D theories such as the Kirchhoff's classical plate theory (CPT) or the shear deformations plate theories (SDTs), various assumptions should be made in order to obtain a 2D formulation. Clearly finding a solution for the plate in 2D formulation is easier. Although in dealing with thin to moderately thick plates the results of these solutions are acceptable, but these simplifying assumptions inherently cause errors for relatively thick plates and therefore may lead to unreliable results. Unlike 2D theories, the 3D ones such as elasticity theory or layerwise theory (LT) do not contain these simplified assumptions. Hence, applying 3D solutions would be more accurate than the ones achieved by the 2D theories. Thus, to eliminate the lack of 2D theories in dealing with thick plates the 3D solutions not only provide realistic and accurate results but also allow further physical insights, which cannot otherwise be estimated by 2D plate theories.

Due to the practical importance as well as theoretical interest, some researches have been performed both on static and dynamic analysis of sector plates. Kobayashi and Turvey [3] investigated an analytical method for the bending response of annular sector Mindlin plates with two radial edges simply supported and presented exact solutions in the form of Levy-type series. Moreover, elastic large deflection of annular sector plates was studied by Salehi and Turvey [4] using dynamic relaxation (DR) finite difference method. After that, Salehi and Shahidi [5] using DR technique along with the central finite differences presented a numerical solution for large deflection behavior of thick isotropic sector plates. Bending analysis of thin sector plates and moderately thick FG sector plates by extended Kantorovich method (EKM) was

* Corresponding author.
E-mail address: kadkhoda@um.ac.ir (M. Kadkhodayan).

http://dx.doi.org/10.1016/j.compositesb.2014.10.048
1359-8368/

Nomenclature

a	inner radius	u	displacement in r direction
b	outer radius	v	displacement in θ direction
$\mathbf{D}$	coefficients of elasticity	W	virtual work
E	elasticity modulus	w	displacement in z direction
$\boldsymbol{F}$	force vector	β	span angle
h	thickness	$\boldsymbol{\varepsilon}$	strain
$\mathbf{K}$	stiffness matrix	$\boldsymbol{\Lambda}$	nodal displacements
$\mathbf{M}$	mass matrix	υ	Poisson ratio
n_r	radial power law exponent	ρ	density
n_z	axial power law exponent	$\boldsymbol{\sigma}$	stress
$\boldsymbol{P}$	surface traction vector	$\boldsymbol{\Phi}$	linear shape functions
T	kinetic energy	Ψ	material properties
$\boldsymbol{U}$	displacement vector		
U	potential energy		

presented by Aghdam et al. [6,7]. Furthermore, Aghdam and Mohammadi [8] investigated the bending analysis of a moderately thick orthotropic sector plate subjected to various loading conditions. The governing equations are based on first order shear deformation theory (FSDT). Mousavi and Tahani [9] developed an analytical solution for the bending of radially functionally graded (RFG) sector plates employing multi-term extended Kantorovich method (MTEKM). The governing equations are derived based on FSDT using the principle of minimum total potential energy. Later, they [10] utilized this method for bending problem of moderately thick composite annular sector plates with general boundary conditions and loadings. An exact analytical approach was used for bending analysis of FG annular sector plates by Jomehzadeh et al. [11], where the governing equations are based on FSDT. Malekzadeh et al. [12] studied the dynamic response of thick laminated annular sector plates with simply supported radial edges subjected to a radially distributed line load which moves along the circumferential direction, where a three-dimensional hybrid method composed of series solution, the layerwise theory and the differential quadrature method in conjunction with the finite difference method was employed. Sharma et al. [13] presented a simple formulation for the nonlinear dynamic analysis of shear-deformable laminated sector plates made up of cylindrically orthotropic layers. The governing equations are based on FSDT.

Moreover, recently several researches have been carried out on the topic of 3D analysis of FGMs. Alibeigloo [14] studied static analysis of simply supported sandwich panel with FGM core subjected to thermo-mechanical loading. Based on theory of elasticity, analytical solutions for the temperature, stress and displacement fields for the sandwich panel with simply supported edges are derived by using the Fourier series expansions along the axial and circumferential directions and statespace technique along the radial direction. Shariyat and Asemi [15] investigated shear buckling analysis of the orthotropic heterogeneous FGM plates. By employing the three dimensional elasticity, results are derived based on principle of minimum potential energy and a non-linear finite element procedure utilizing a Galerkin-type 3D cubic B-spline solution algorithm. Exact solution of steady state thermo-elastic problem of three dimensional circular plate made of FGM is developed by Jabbari et al. [16]. A full analytical method was used and the boundary condition was assumed as simply supported. Asemi et al. [17,18] studied buckling and post buckling of FG annular sector plates fully or partially supported on Winkler elastic foundation subjected to uniform in-plane compressive loads based on three dimensional theory of elasticity. The governing equations were developed based on the principle of minimum total potential energy and solved based on finite element orthogonal integral equations. Hosseini-Hashemi et al. [19] presented exact closed-form solutions of 3D elasticity theory to study both in-plane and out-of-plane free vibrations for thick functionally graded simply supported rectangular plates. The 3D elasto-dynamic equations are written in terms of some suitable independent functions satisfying ordinary differential equations. In each case, the obtained ordinary differential equations are analytically solved and boundary conditions are satisfied. A combined spline finite strip and state space approach is introduced to obtain threedimensional solutions of laminated composite plates with general boundary conditions by Attallah et al. [20]. Spline and linear polynomial functions are used, respectively, as the shape functions in the longitudinal and transverse directions of the strips. Cheng and Batra [21] obtained a new solution in closed form for the thermomechanical deformations of an isotropic linear thermoelastic functionally graded elliptic plate rigidly clamped at the edges. They found that the through-thickness distributions of the in-plane displacements and transverse shear stresses in a functionally graded plate do not agree with those assumed in classical and shear deformation plate theories. Na and Kim [22] investigated the three dimensional thermal buckling analysis for functionally graded materials. The finite element model is adopted by using an 18-node solid element to analyze more accurately the variation of material properties and temperature field in the thickness direction. Using a three-dimensional layerwise-finite element method, the free vibration of thick laminated circular and annular plates supported on the elastic foundation was studied by Malekzadeh et al. [23]. The discretized governing equations were derived using the Hamilton's principle in conjunction with the layerwise theory in the thickness direction, the finite element in the radial direction and trigonometric function in the circumferential direction, respectively. Setoodeh et al. [24] studied the transient dynamic and free vibration analysis of FG axisymmetric truncated conical shells with non-uniform thickness. Employing the displacement-based layerwise theory in conjunction with the Hamilton's principle, the transversely discretized equations of motion were obtained and the differential quadrature method (DQM) was used to discretize the resulting equations in the axial direction. Andakhshideh and Tahani [25] investigated analytically the inter-laminar stresses near free edges of finite length general composite laminates subjected to axial and shearing loads. Employing three-dimensional multi-term extended Kantorovich method in conjunction with the principle of minimum total potential energy, three systems of coupled ordinary differential equations were obtained. Then an iterative procedure was established to achieve analytical solution. Maturi et al. [26] investigated the static and free vibration analyses of sandwich plates using collocation with radial basis functions and a new layerwise

theory with independent rotations in each layer and thickness stretching. A three dimensional elasticity approach is used to develop a general free vibration and buckling analysis of composite plates with elastic restrained edges by Setoodeh and Karami [27]. Roque et al. [28] modeled symmetric composite plates with the use of trigonometric layerwise deformation theory and a meshless discretization method based on global multiquadric radial basis functions. They revealed that the use of trigonometric layerwise deformation theory discretized with multiquadrics provides very good solutions for composite plates and excellent solutions for sandwich plates. Shariyat and Alipour [29,30] presented the stress analysis of FGM circular and annular plates. The governing equations are derived based on the zigzag-elasticity formulation.

Literature review denotes that although a few works have been performed on transient analysis of sector plates; but transient analysis of FG sector plate has not been taken into consideration yet. Besides, the vast majority of studies deal with 2D plate theories while the application of these theories to thick structures can cause considerable errors. Moreover, the material properties have been assumed to have a smooth variation in one direction. Conventional FGMs may also not to be so effective in such design problems since all outer surface of the body will have the same composition distribution. Therefore, variation of volume fraction in two directions has a higher capability to reduce the mechanical, thermal and residual stresses and leads to a more flexible design than 1D-FGMs. Some studies have been carried out about static and dynamic analyses of structures made of 2D-FGMs [31–33]. Furthermore, analytical or semi-analytical solutions are available only through a number of problems with simple boundary conditions. Hence, for the first time, the static and dynamic response of 2D-FG thick sector plate with general boundary conditions based on 3D theory of elasticity is presented.

The purpose of this paper is to investigate the static and dynamic responses of thick 2D-FG sector plates. The Young modulus and density of the plate is varied through both radial and axial directions with power law functions and the Poisson's ratio is assumed to be constant. The governing equations are derived based on Hamilton's principle and Rayleigh–Ritz method. To solve the time dependent equations, Newmark direct integration method with suitable time steps is used. The static and transient responses of sector plates for different material gradient indices, boundary conditions and thickness to radius ratios of sector plates are computed and compared.

The difficulty in obtaining analytical solutions for the response of graded material systems comes from the dispersion of the heterogeneous material systems. Therefore, analytical or semi-analytical solutions are available only through a number of problems with simple boundary conditions. Thus, in order to find the solution for a thick 2D-FG sector plate subjected to static and dynamic loading with general boundary conditions, powerful numerical methods such as GFEM are needed. The graded finite elements, which incorporate the material property gradient at the element level (material properties in each element are interpolated using linear shape functions), have been employed a generalized isoparametric formulation. Some works can be found in the literature on modeling of non-homogenous structures by using GFEM [34–36]. In these researches, it is shown that the conventional FEM formulation causes a discontinuous stress field, while the graded elements give a continuous and smooth variation. Moreover, in the conventional FEM formulations, when the material properties vary through the thickness, several elements need to be considered in the thickness in order to obtain converged results. But by employing GFEM, the number of elements in the thickness reduces considerably. Thus, the run-time and calculational efficiency in this approach do not differ significantly in comparison with the 2D approaches. Accordingly, the desired results are obtained without too much redundant computational costs.

2. Mathematical formulation

2.1. Distribution of material properties in 2D-FG sector plate

Consider a thick sector plate of inner radius a, outer radius b, thickness h and span angle β subjected to transverse loading. The geometry and coordinate system of the sector plate is shown in Fig. 1.

2D-FGMs are usually made by smooth variation of three or four distinct material phases in which one or two of them are ceramics and the others are metal alloy phases. Since powerful improvements in fabrication and processing methods have been developed, by utilizing computer aided manufacturing processes, producing FGMs with two and three dimensional gradients is possible. The upper surface of the sector plate is made of two distinct ceramics and the lower surface consists of two metals. The volume fractions of the components vary continuously through the r and z directions in a predefined composition profile. The volume fraction distribution function of each material can be expressed as:

$$V_{m1}(r,z) = \left[1 - \left(\frac{r-a}{b-a}\right)^{n_r}\right]\left[1 - \left(\frac{z}{h}\right)^{n_z}\right] \tag{1}$$

$$V_{m2}(r,z) = \left(\frac{r-a}{b-a}\right)^{n_r}\left[1 - \left(\frac{z}{h}\right)^{n_z}\right] \tag{2}$$

$$V_{c1}(r,z) = \left[1 - \left(\frac{r-a}{b-a}\right)^{n_r}\right]\left(\frac{z}{h}\right)^{n_z} \tag{3}$$

$$V_{c2}(r,z) = \left(\frac{r-a}{b-a}\right)^{n_r}\left(\frac{z}{h}\right)^{n_z} \tag{4}$$

where $m1$, $m2$, $c1$ and $c2$ denote the first and the second metal and ceramic, respectively. n_r and n_z are non-negative volume fraction exponents through the r and z directions. For instant, the volume fraction distributions of the second metal (V_{m2}) for the typical values of $n_r = 2$ and $n_z = 3$ is shown in Fig. 2. It is assumed that $a = 0.4$ m, $b = 1$ m and $h = 0.15$ m. Material properties at each point can be obtained by using the linear rule of mixtures; therefore the material property Ψ such as modulus of elasticity or mass density in the 2D-FG sector plate is calculated by linear combination of volume fractions and material properties of the constituent materials as:

$$\Psi = \Psi_{c1}\, V_{c1} + \Psi_{c2}\, V_{c2} + \Psi_{m1}\, V_{m1} + \Psi_{m2}\, V_{m2} \tag{5}$$

The basic constituents of the 2D-FG sector plate are presented in Table 1. The variation of a material property such as modulus of elasticity based on the mentioned approach for the typical values of $n_r = 2$ and $n_z = 3$ is depicted in Fig. 3. It should be noted that the Poisson's ratio is assumed to be constant through the body.

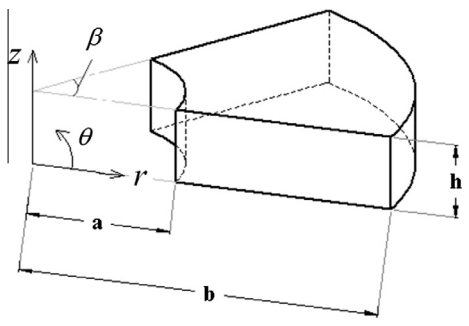

Fig. 1. Geometry of thick sector plate.

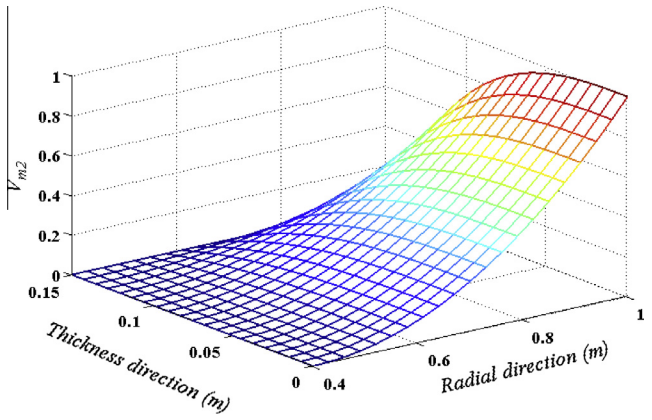

Fig. 2. Volume fraction distribution of $m2$ with $n_r = 2$ and $n_z = 3$.

Table 1
Basic constituents of the 2D-FG sector plate.

Constituents	E (GPa)	ρ (kg/m^3)	υ
$m1$	115	4515	0.3
$m2$	70	2715	0.3
$c1$	440	3210	0.3
$c2$	380	3800	0.3

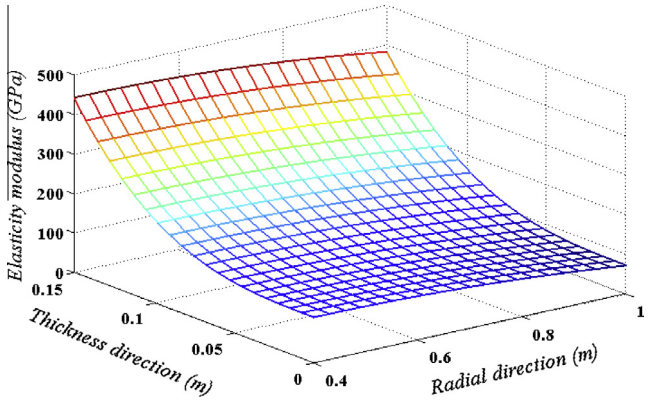

Fig. 3. Distribution of elasticity modulus with $n_r = 2$ and $n_z = 3$.

2.2. Governing equations

Governing equations may be obtained based on the Hamilton's principle:

$$\int_{t_1}^{t_2} \delta I \; dt = \int_{t_1}^{t_2} \delta(U - W - T) \; dt = 0 \tag{6}$$

where U, W and T are potential energy, work done by external forces and kinetic energy, respectively. These functions and their variations are:

$$U = \frac{1}{2} \iiint_{\Omega} \boldsymbol{\varepsilon}^T \cdot \boldsymbol{\sigma} \; d\Omega \tag{7}$$

$$\delta U = \iiint_{\Omega} \delta\boldsymbol{\varepsilon}^T \cdot \boldsymbol{\sigma} \; d\Omega \tag{8}$$

$$W = \int_{\Gamma} \int \boldsymbol{P}^T \cdot \boldsymbol{U} \; d\Gamma \tag{9}$$

$$\delta W = \int_{\Gamma} \int \boldsymbol{P}^T \cdot \delta\boldsymbol{U} \; d\Gamma \tag{10}$$

$$T = \frac{1}{2} \iiint_{\Gamma} \rho\dot{\boldsymbol{U}}^T \cdot \dot{\boldsymbol{U}} d\Omega \tag{11}$$

$$\delta T = \iiint_{\Omega} \rho\dot{\boldsymbol{U}}^T \cdot \delta\dot{\boldsymbol{U}} d\Omega \tag{12}$$

where Ω and Γ are the volume and area of the domain under consideration, ρ is the mass density that depends on r and z coordinates and $\boldsymbol{P}$ is the vector of surface traction and in the current work is defined as:

$$\boldsymbol{P} = \{0 \;\; 0 \;\; p_z\}^T \tag{13}$$

Substituting Eqs. (7)–(12) in Hamilton's principle, applying side conditions $\delta\boldsymbol{U}|_{t_1,t_2} = 0$ and using part integration:

$$\iiint_{\Omega} \delta\boldsymbol{\varepsilon}^T \cdot \boldsymbol{\sigma} d\Omega + \iiint_{\Omega} \rho\ddot{\boldsymbol{U}}^T \cdot \delta\boldsymbol{U} \; d\Omega = \int_{\Gamma} \int \boldsymbol{P}^T \cdot \delta\boldsymbol{U} \; d\Gamma \tag{14}$$

The stress–strain relation from the Hook's law in the matrix form is as [37]:

$$\boldsymbol{\sigma} = \mathbf{D} \cdot \boldsymbol{\varepsilon} \tag{15}$$

where the stress and strain components and the coefficients of elasticity $\mathbf{D}$, are as following [37]:

$$\boldsymbol{\sigma} = \{\sigma_r \quad \sigma_\theta \quad \sigma_z \quad \sigma_{\theta z} \quad \sigma_{rz} \quad \sigma_{r\theta}\}^T \tag{16}$$

$$\boldsymbol{\varepsilon} = \{\varepsilon_r \quad \varepsilon_\theta \quad \varepsilon_z \quad \gamma_{\theta z} \quad \gamma_{rz} \quad \gamma_{r\theta}\}^T \tag{17}$$

$$\mathbf{D} = \frac{E(r,z)}{(1+\upsilon)(1-2\upsilon)} \begin{bmatrix} 1-\upsilon & \upsilon & \upsilon & 0 & 0 & 0 \\ \upsilon & 1-\upsilon & \upsilon & 0 & 0 & 0 \\ \upsilon & \upsilon & 1-\upsilon & 0 & 0 & 0 \\ 0 & 0 & 0 & \frac{1-2\upsilon}{2} & 0 & 0 \\ 0 & 0 & 0 & 0 & \frac{1-2\upsilon}{2} & 0 \\ 0 & 0 & 0 & 0 & 0 & \frac{1-2\upsilon}{2} \end{bmatrix} \tag{18}$$

in which υ denotes the Poisson's ratio that is assumed to be constant and E is the Young's modulus of elasticity that depends on r and z coordinates.

The strain–displacement equations based on the linear theory of elasticity in cylindrical coordinate are [37]:

$$\begin{aligned} &\varepsilon_r = \frac{\partial u}{\partial r}, \;\; \varepsilon_\theta = \frac{1}{r}\left(u + \frac{\partial v}{\partial \theta}\right), \;\; \varepsilon_z = \frac{\partial w}{\partial z} \\ &\gamma_{\theta z} = \frac{\partial v}{\partial z} + \frac{1}{r}\frac{\partial w}{\partial \theta}, \;\; \gamma_{rz} = \frac{\partial u}{\partial z} + \frac{\partial w}{\partial r}, \;\; \gamma_{r\theta} = \frac{1}{r}\frac{\partial u}{\partial \theta} + \frac{\partial v}{\partial r} - \frac{v}{r} \end{aligned} \tag{19}$$

where u, v and w are radial, circumferential and axial components of displacement, respectively. Eq. (19) can be formulated in the matrix form as:

$$\boldsymbol{\varepsilon} = \boldsymbol{\mathcal{L}} \cdot \boldsymbol{U} \tag{20}$$

in which $\boldsymbol{U}$ is displacement vector and $\boldsymbol{\mathcal{L}}$ is a matrix containing partial differentiating equations as follow:

$$\boldsymbol{U} = \{u \quad v \quad w\}^T \tag{21}$$

$$\boldsymbol{\mathcal{L}} = \begin{bmatrix} \partial_r & 1/r & 0 & 0 & \partial_z & 1/r\partial_\theta \\ 0 & 1/r\partial_\theta & 0 & \partial_z & 0 & \partial_r - 1/r \\ 0 & 0 & \partial_z & 1/r\partial_\theta & \partial_r & 0 \end{bmatrix}^T \tag{22}$$

The sector plate is subjected to transverse loading and the boundary conditions used in this study are defined as follow:

$$\text{CCCC}: \begin{cases} r = a, b \\ \theta = 0, \beta \end{cases} \rightarrow |u = v = w = 0$$

$$\text{SSSS}: \begin{cases} r = a, b \rightarrow |v = w = 0 \\ \theta = 0, \beta \rightarrow |u = w = 0 \end{cases}$$

$$\text{CSCS}: \begin{cases} r = a, b \rightarrow |u = v = w = 0 \\ \theta = 0, \beta \rightarrow |u = w = 0 \end{cases}$$

$$\text{FSFS}: \{\theta = 0, \beta \rightarrow |u = w = 0 \tag{23}$$

2.3. Graded finite element modeling

In order to solve the governing equations, the GFEM is employed. In this method, in addition to displacement field, the heterogeneity of the material properties of the FGM may also be determined based on their nodal values. In this regard, shape functions similar to those of the displacement field may be used. Therefore, a GFEM is used to effectively trace smooth variations of the material properties at the element level. Using the graded elements for modeling of gradation of the material leads to more accurate results than dividing the solution domain into homogenous elements.

The thick sector plate is divided into a number of 8-node linear elements. The element displacements in three directions are approximated as follows:

$$\boldsymbol{U}^{(e)} = \boldsymbol{\Phi} \cdot \boldsymbol{\Lambda}^{(e)} \tag{24}$$

where $\boldsymbol{\Phi}$ is the matrix of linear shape functions in cylindrical coordinate and $\boldsymbol{\Lambda}^{(e)}$ is the element nodal displacement vector that are as:

$$\boldsymbol{\Phi} = \begin{bmatrix} \Phi_1 & 0 & 0 & \cdots & \Phi_8 & 0 & 0 \\ 0 & \Phi_1 & 0 & \cdots & 0 & \Phi_8 & 0 \\ 0 & 0 & \Phi_1 & \cdots & 0 & 0 & \Phi_8 \end{bmatrix} \tag{25}$$

$$\boldsymbol{\Lambda}^{(e)} = \{U_1 \quad V_1 \quad W_1 \quad \cdots \quad U_8 \quad V_8 \quad W_8\}^T \tag{26}$$

The components of $\boldsymbol{\Phi}$ are given in Appendix A.

To treat the material inhomogeneity by using the GFEM, it may be written that:

$$\Psi^{(e)} = \sum_{i=1}^{8} \Psi_i \Phi_i \tag{27}$$

where $\Psi^{(e)}$ is the material property of the element.

Substituting Eq. (24) in Eq. (20) gives the element strain matrix as:

$$\boldsymbol{\varepsilon}^{(e)} = \mathbf{B} \cdot \boldsymbol{\Lambda}^{(e)} \tag{28}$$

where

$$\mathbf{B} = \boldsymbol{\mathcal{L}} \cdot \boldsymbol{\Phi}^{(e)} \tag{29}$$

By imposing Eqs. (15), (24) and (28) into Hamilton's principle (Eq. (14)) for each element, it can be achieved that:

$$\delta\boldsymbol{\Lambda}^{(e)^T} \left\{ \iiint_{\Omega^{(e)}} \rho \boldsymbol{\Phi}^T \cdot \boldsymbol{\Phi} d\Omega \right\} \ddot{\boldsymbol{\Lambda}}^{(e)} + \delta\boldsymbol{\Lambda}^{(e)^T} \left\{ \iiint_{\Omega^{(e)}} \mathbf{B}^T \cdot \mathbf{D} \cdot \mathbf{B} d\Omega \right\} \boldsymbol{\Lambda}^{(e)}$$
$$= \delta\boldsymbol{\Lambda}^{(e)^T} \int \int_{\Gamma^{(e)}} \boldsymbol{\Phi}^T \cdot \boldsymbol{P} d\Gamma \tag{30}$$

Since $\delta\boldsymbol{\Lambda}^{(e)^T}$ is the variation of the nodal displacements and is arbitrary, it can be omitted from Eq. (30) and in a compact form it can be formulated as:

$$\mathbf{M}^{(e)} \ddot{\boldsymbol{\Lambda}}^{(e)} + \mathbf{K}^{(e)} \boldsymbol{\Lambda}^{(e)} = \boldsymbol{F}^{(e)} \tag{31}$$

where the characteristic matrices are defined as:

$$\mathbf{M}^{(e)} = \iiint_{\Omega^{(e)}} \rho \boldsymbol{\Phi}^T \cdot \boldsymbol{\Phi} \, d\Omega \tag{32}$$

$$\mathbf{K}^{(e)} = \iiint_{\Omega^{(e)}} \mathbf{B}^T \cdot \boldsymbol{D} \cdot \boldsymbol{B} \, d\Omega \tag{33}$$

$$\boldsymbol{F}^{(e)} = \iint_{\Gamma^{(e)}} \boldsymbol{\Phi}^T \cdot \boldsymbol{P} \, d\Gamma \tag{34}$$

Due to dependency of $\mathbf{D}$ and ρ to the r and z coordinates, for obtaining the characteristic matrices for each element, numerical integration using 8-point Gauss–Legendre technique should be applied [38]. Now by assembling the element matrices and imposing the boundary conditions, the global equations of motion for the 2D-FG sector plate can be written as:

$$\mathbf{M}\ddot{\boldsymbol{\Lambda}} + \mathbf{K}\boldsymbol{\Lambda} = \boldsymbol{F} \tag{35}$$

In order to solve Eq. (35) in the space and time domains different numerical methods can be employed. In the current work, Newmark's numerical integration method with suitable time steps is used. Newmark integration parameters [38] are taken as $\gamma = 1/2$ and $\beta = 1/4$ which lead to a constant average acceleration. This choice of parameters corresponds to the trapezoidal rule which is unconditionally stable in linear analyses. Moreover, in the case of static analysis, Eq. (35) is reduced to:

$$\mathbf{K}\boldsymbol{\Lambda} = \boldsymbol{F} \tag{36}$$

Once the finite element equations are established, the displacements and stresses would be found by Eqs. (35), (36) and (15), respectively. It should be noted that calculated stresses are often most accurate at Gauss points. Thus, in this research, stresses at nodes are obtained by extrapolation or interpolation from Gauss point values.

3. Numerical results and discussions

3.1. Convergence study

In order to examine the efficiency and accuracy of the presented FE code, the results should be compared with an exact 3D solution. Since there is no study available in the literature for 3D solution of sector plates, the results are compared with the available exact 3D solution for FG rectangular plate given by Kashtalyan [39]. For this purpose, by considering very large values for a and b together with a very small value for β, the governing equations and presented solution procedure may also be employed for bending analysis of rectangular plates. The relationship between length and width of the rectangular plate can be considered as $\beta(a+b)/2$ and $b-a$, respectively. First, the effects of mesh density on the obtained results for an FG square plate with simply supported boundary conditions under sinusoidal load with length to thickness ratio of 3, are examined and presented in Fig. 4. Numerous mesh densities containing $4 \times 4 \times 4$, $6 \times 6 \times 6$, …, $22 \times 22 \times 22$ regularly placed along the r, θ and z directions are considered. In which w^* refers to the exact solution of the centroid deflection obtained by Kashtalyan [39]. According to this figure, it is observed that as the mesh density increases more than $18 \times 18 \times 18$, the normalized deflection (w/w^*) does not vary considerably. Moreover, the influence of mesh density along the plate thickness direction is depicted in Fig. 5. In this figure, various mesh densities containing $18 \times 18 \times 4$, $18 \times 18 \times 6$, …, $18 \times 18 \times 14$ have been considered. It

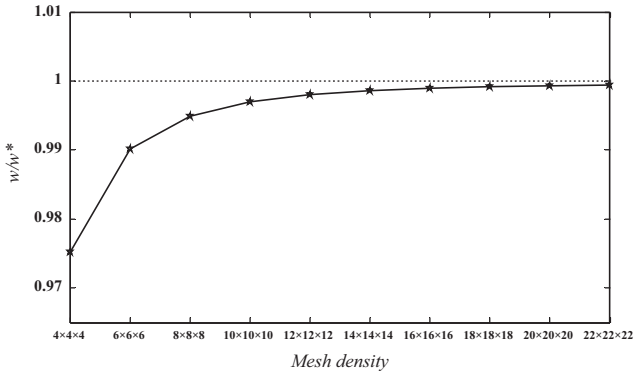

Fig. 4. Convergence of the results for the normalized deflection with various mesh densities.

can be observed that considering 14 meshes along the plate thickness direction led to the exact solution. Therefore, to obtain the solutions in the presented study, the mesh density is assumed to be $18 \times 18 \times 14$ (4536 elements, 5415 nodes and 16,245 degrees of freedom).

3.2. Verification

In order to verify the prepared 3D GFEM code for static and dynamic analyses of the 2D-FG sector plate, three comparison studies are performed as follow:

Sample 1: As a first case study, the results of moderately thick FG sector plate can be used [7]. Material distribution is assumed to be as 1D-FG which varies in thickness direction from pure metal (E_m = 70 GPa, υ_m = 0.3) to pure ceramic (E_c = 380 GPa, υ_c = 0.3) with a simple power law function. The boundary condition is full clamped at all side edges, the sector plate is under uniform pressure (p) and the geometry is defined as:

$$a = 3 \text{ m},\ b = 5 \text{ m},\ h = 0.3 \text{ m},\ \beta = \pi/4 \tag{37}$$

The comparison of normalized deflection ($w^{**} = wE_c h^3/pb^4$) along the centerline ($r = (a+b)/2,\ \theta$) with the published data for different volume fraction exponents is shown in Fig. 6 and a good agreement between them is observed.

Sample 2: In the second example, a comparison study is accomplished for dimensionless deflection ($\bar{w} = wE_m h^3/12(1-\upsilon^2)pb^4$) and shear stress ($\bar{\tau}_{rz} = \tau_{rz}/p$) of bending analysis in a simply supported FG solid sector plate which its solution is presented by Sahraee [40], where the governing equations are based on Levinson plate theory (LPT). The thickness to radius ratio is taken as 0.1 and

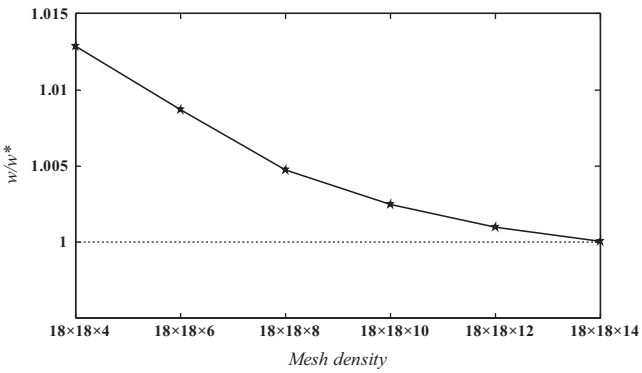

Fig. 5. Convergence of the results for the normalized deflection with various mesh densities along the plate thickness.

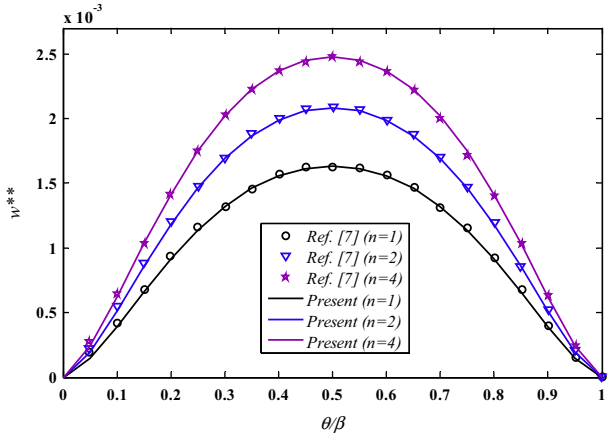

Fig. 6. Variation of the normalized deflection (w^{**}) along the centerline for different volume fraction exponent n compared with [7].

the ratio of Young's modulus of metal component to ceramic component is assumed to be 0.4636. The results for different volume fraction exponents are demonstrate in Table 2, where the present results are in a good agreement with the other solution.

Sample 3: As a final part of verification, the dynamic behavior of an isotropic sector plate subjected to impact loading with clamped boundary condition is calculated and compared with the results of commercial FEA software [41]. The geometry, material and loading function are assumed to be as:

$$a = 0.4 \text{ m},\ b = 1 \text{ m},\ h = 0.1 \text{ m},\ \beta = \pi/4 \quad E = 70 \text{ GPa}\ \upsilon = 0.3 \tag{38}$$

$$p_z(t) = \begin{cases} P_0 t & t \leqslant t_0 \\ 0 & t > t_0 \end{cases} \tag{39}$$

where P_0 and t_0 are assumed to be as 2×10^4 MPa and 5×10^{-4} s, respectively. The comparison of time histories of centroid deflection and axial stress with the Abaqus' results are depicted in Figs. 7 and 8. It is obvious that the present solutions are in good consistency with the software results.

3.3. Static analysis

Consider a 2D-FG thick sector plate with inner radius of a = 0.4 m, outer radius of b = 1 m, span angle of $\beta = \pi/3$ and subjected to uniform pressure of P_0 = 10 MPa. Constituent materials are two distinct ceramics and two distinct metals described in Table 1.

First, the effect of power law exponents (n_r, n_z) on the static response of the sector plate is studied. The thickness to radius ratio of the sector plate and the boundary conditions are assumed to be h/b = 0.1 and CCCC, respectively. Fig. 9 shows the variation of central deflection along the radial direction at $z = 0$ and $\theta = \beta/2$ for different power law exponents. According to this figure, deflection increase as n_z increases and n_r decreases, this behavior

Table 2
Dimensionless deflection and shear stress for different volume fraction exponent compared with [40].

n	$\bar{w}$ (0.75b, $\pi/4$, 0)		$\bar{\tau}_{rz}$ (0.75 b, $\pi/6$, 0)	
	Present	Ref. [40]	Present	Ref. [40]
0	1.1721	1.1613	−0.6691	−0.6609
2	1.3112	1.2946	−0.6864	−0.6789
5	2.1893	2.1758	−0.7007	−0.6916

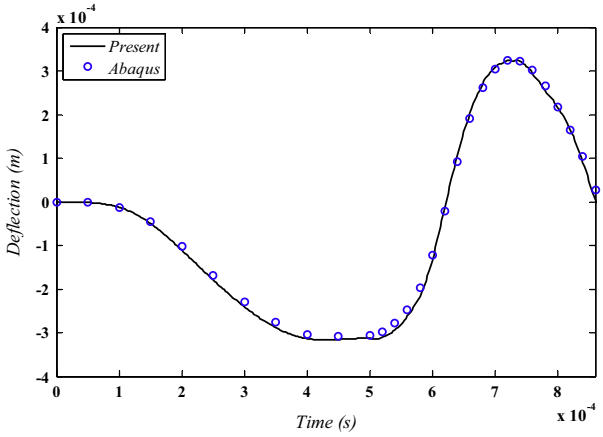

Fig. 7. Time history of centroid deflection compared with Abaqus.

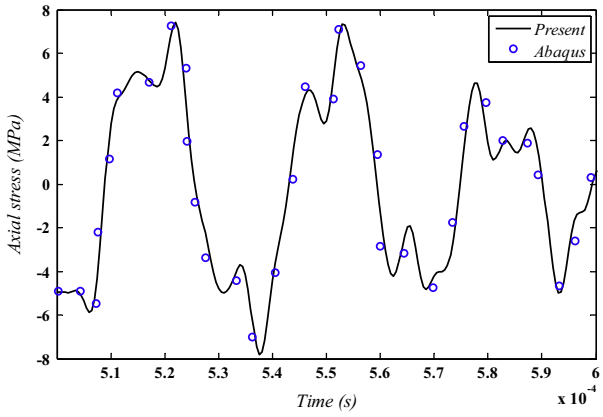

Fig. 8. Time history of centroid axial stress compared with Abaqus.

is due to the resulting decrease in the modulus of elasticity. Moreover, the influence of changing n_z on the deflection is more noticeable than changing n_r. The variations of radial stress through the radial direction at $z = 0$ and $\theta = \beta/2$, and circumferential stress along the centerline at $z = 0$ and $r = (a + b)/2$ for different power law exponents are illustrated in Figs. 10 and 11, respectively. It is seen that by increasing n_r and n_z, the radial and circumferential stresses rises, in which changing n_z has a more effect on variation of stresses rather than n_r. Furthermore, Fig. 12 demonstrates the variation of radial stress through the thickness direction at $r = (a + b)/2$ and $\theta = \beta/2$ for different power law exponents. This figure shows that there is a compression at the top surface and tension at the bottom surface, in which the magnitude of radial stress at the top surface (ceramic) is significantly larger than that of the bottom surface (metal). Moreover, the neutral plane (where σ_r vanishes) goes upper with increasing of power law exponent.

Now, the effect of thickness to radius ratio (h/b) on the static response of the sector plate is investigated. The power law exponents and boundary conditions are assumed to be $n_r = 2$, $n_z = 3$ and CCCC, respectively. Fig. 13 displays the variation of central deflection through the radial direction at $z = 0$ and $\theta = \beta/2$ for different thickness to radius ratios. According to this figure, thickness to radius ratio has a high influence on the deflection of the sector plate. The variations of radial stress through the radial direction at $z = 0$ and $\theta = \beta/2$, and circumferential stress along the centerline at $z = 0$ and $r = (a + b)/2$ for different thickness to radius ratios are illustrated in Figs. 14 and 15, respectively. From these figures, it can be observed that by tripling the thickness to radius ratio of the plate, the stresses may be reduced up to 90%. Moreover, Fig. 16 shows the variation of radial stress versus non-dimensional thickness (z/h) at $r = (a + b)/2$ and $\theta = \beta/2$ for different thickness to radius ratios. From this figure, the non-dimensional position of neutral plane remains unchanged when thickness to radius ratio varies. Furthermore, the effect of boundary condition on the static behavior of the sector plate for different thickness to radius ratios and power law exponents is tabulated in Table 3. The results show that the influence of boundary condition on deflection is more significant than that of stresses.

3.4. Dynamic analysis

Consider the 2D-FG sector plate of the previous section once again. As already mentioned, it is assumed that the sector plate is fabricated from two distinct ceramics and metals as described in Table 1. The sector plate is subjected to an impact loading at the top surface. The loading function is assumed as:

$$p_z(t) = \begin{cases} P_0 \sin\left(\frac{\pi t}{t_0}\right) & t \leqslant t_0 \\ 0 & t > t_0 \end{cases} \tag{40}$$

where P_0 and t_0 are loading constants that are assumed to be as 10 MPa and 5×10^{-4} s, respectively. Variation of the lateral impact pressure with time is displayed in Fig. 17. According to this figure, the sector plate is excited by unloading in $t_0 = 5 \times 10^{-4}$ s. It is obvious that after unloading, a transient vibration which is affected by

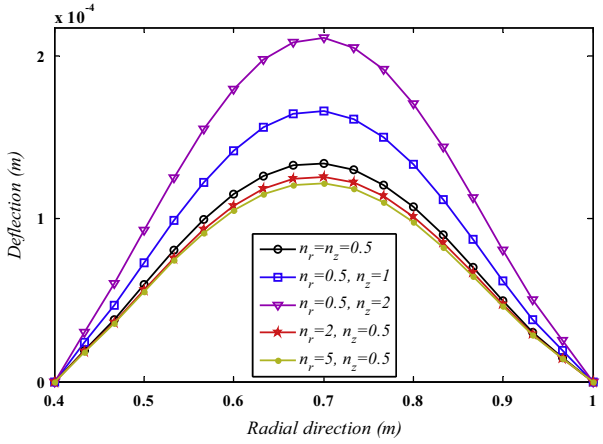

Fig. 9. Variation of central deflection through the radial direction at $z = 0$ and $\theta = \beta/2$ for different power law exponents.

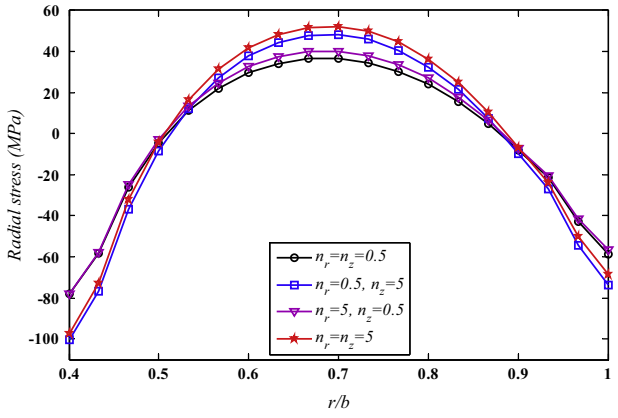

Fig. 10. Variation of radial stress through the radial direction at $z = 0$ and $\theta = \beta/2$ for different power law exponents.

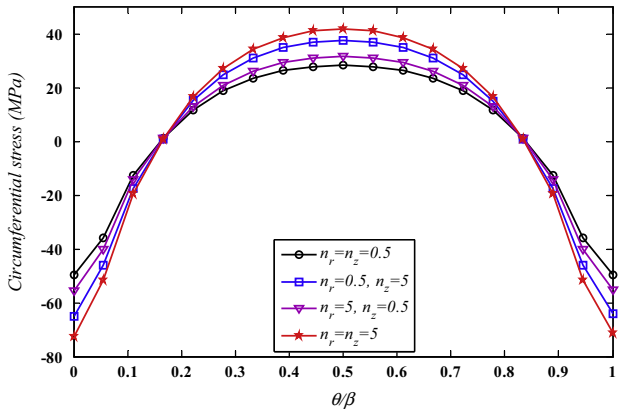

Fig. 11. Variation of circumferential stress along the centerline at $z = 0$ and $r = (a + b)/2$ for different power law exponents.

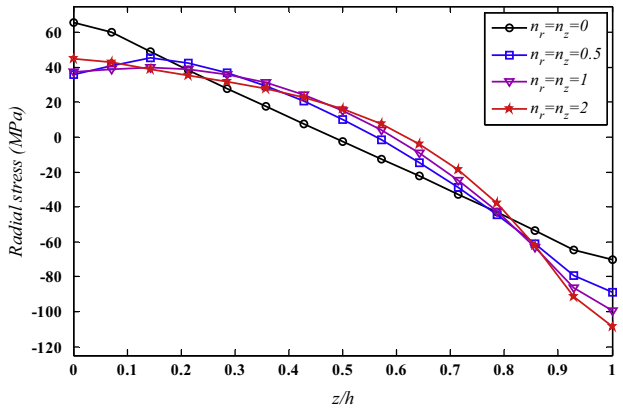

Fig. 12. Variation of radial stress through the thickness direction at $r = (a + b)/2$ and $\theta = \beta/2$ for different power law exponents.

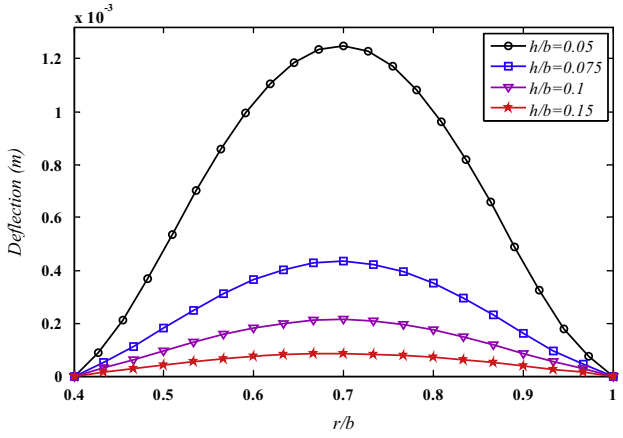

Fig. 13. Variation of central deflection through the radial direction at $z = 0$ and $\theta = \beta/2$ for different thickness to radius ratios.

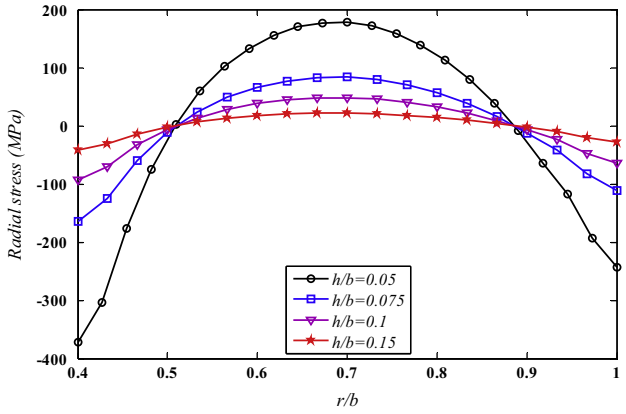

Fig. 14. Variation of radial stress through the radial direction at $z = 0$ and $\theta = \beta/2$ for different thickness to radius ratios.

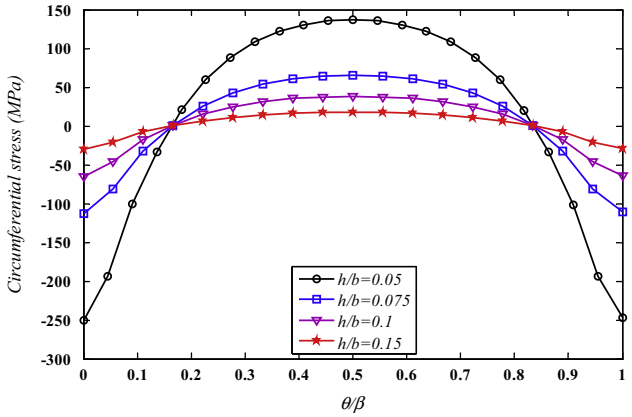

Fig. 15. Variation of circumferential stress along the center line at $z = 0$ and $r = (a + b)/2$ for different thickness to radius ratios.

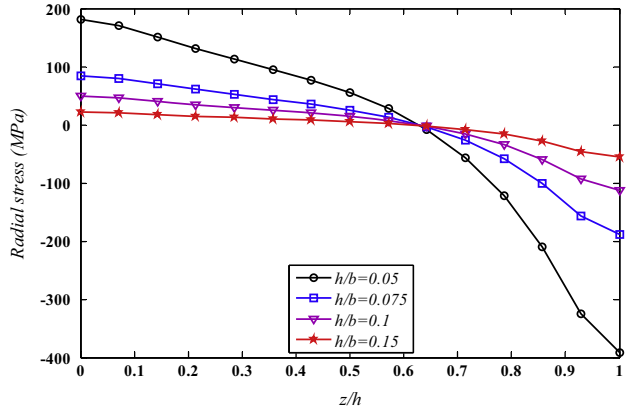

Fig. 16. Variation of radial stress through the thickness direction at $r = (a + b)/2$ and $\theta = \beta/2$ for different thickness to radius ratios.

the wave propagation, reflection and interference would be occurred. The three dimensional transient analysis for different values of the power law exponents and thickness to radius ratio are presented and discussed as following.

Fig. 18 shows the time history of the central deflection of the sector plate for different power law exponents with thickness to radius ratio of $h/b = 0.1$ and CCCC boundary condition. According to this figure, by increasing the power law exponents, the amplitude of vibrations increases. The time history of the stress components σ_z and σ_r at the center point of the sector plate $(r = (a + b)/2,\ \theta = \beta/2,\ z = h/2)$ after unloading for different power law exponents with thickness to radius ratio of $h/b = 0.1$ and CCCC boundary condition are illustrated in Figs. 19 and 20. These results reveal how the propagation of the stress wave following the unloading is highly affected by the variation of volume fraction of the constituent materials in two directions. In which, by

Table 3
Deflection and stresses of the center point for different boundary conditions.

B.C.	h/b	n_r	n_z	$10^5 \times w$ (m)	σ_r (MPa)	σ_θ (MPa)	σ_z (MPa)
CCCC	0.05	0.5	0.5	−82.253	42.416	32.496	−4.592
		0.5	5	−154.950	45.793	34.971	−4.374
		5	0.5	−74.606	39.258	30.195	−4.709
		5	5	−130.415	42.649	32.656	−4.559
	0.1	0.5	0.5	−13.874	10.008	7.647	−4.775
		0.5	5	−27.942	11.246	8.572	−4.582
		5	0.5	−12.616	9.152	7.014	−4.875
		5	5	−23.448	10.268	7.890	−4.744
	0.15	0.5	0.5	−5.540	3.559	2.679	−4.803
		0.5	5	−11.771	4.359	3.252	−4.637
		5	0.5	−5.049	3.158	2.373	−4.899
		5	5	−9.858	3.815	2.879	−4.802
SSSS	0.05	0.5	0.5	−261.953	96.460	74.401	−4.508
		0.5	5	−480.548	102.233	78.480	−4.353
		5	0.5	−234.347	87.821	68.983	−4.659
		5	5	−395.875	91.976	73.045	−4.564
	0.1	0.5	0.5	−37.185	25.219	19.084	−4.761
		0.5	5	−70.828	26.706	20.162	−4.589
		5	0.5	−33.344	22.951	17.682	−4.875
		5	5	−58.376	23.903	18.741	−4.766
	0.15	0.5	0.5	−12.419	11.192	8.223	−4.792
		0.5	5	−24.657	11.775	8.660	−4.619
		5	0.5	−11.159	10.158	7.596	−4.899
		5	5	−20.333	10.431	8.0152	−4.797
CSCS	0.05	0.5	0.5	−108.048	54.271	33.331	−4.745
		0.5	5	−202.794	58.424	35.508	−4.445
		5	0.5	−98.886	50.727	31.265	−4.874
		5	5	−173.324	55.247	33.639	−4.657
	0.1	0.5	0.5	−17.870	13.387	9.379	−4.806
		0.5	5	−35.834	14.843	10.025	−4.594
		5	0.5	−16.381	12.436	8.811	−4.912
		5	5	−30.499	13.851	9.518	−4.770
	0.15	0.5	0.5	−6.985	5.252	4.489	−4.813
		0.5	5	−14.751	6.127	4.752	−4.635
		5	0.5	−6.407	4.812	4.214	−4.914
		5	5	−12.506	5.573	4.505	−4.814
FSFS	0.05	0.5	0.5	−1745.719	12.411	272.707	−4.263
		0.5	5	−3276.701	8.395	294.586	−3.985
		5	0.5	−1576.656	12.258	257.292	−4.378
		5	5	−2738.262	10.528	282.206	−4.159
	0.1	0.5	0.5	−266.672	2.235	80.821	−4.670
		0.5	5	−500.926	0.528	86.225	−4.446
		5	0.5	−240.616	2.393	76.241	−4.753
		5	5	−417.242	1.378	82.494	−4.577
	0.15	0.5	0.5	−86.793	0.759	38.028	−4.772
		0.5	5	−164.366	−0.375	40.213	−4.579
		5	0.5	−78.261	0.874	35.866	−4.848
		5	5	−136.604	0.039	38.428	−4.697

increasing the power law exponents, the amplitude of the vibrations rises while the velocity of stress wave propagation decreases.

Furthermore, the effect of thickness to radius ratio on the dynamic response of the 2D-FG sector plate with $n_r = 2$, $n_z = 3$ and CCCC boundary condition is demonstrated in Figs. 21–23. From these figures, it can be found that increasing the thickness to radius ratio leads to higher stress wave propagation velocity and lower amplitude of vibrations. Moreover, nonzero initial phases and many wavelets appear on the wave curves of stresses as a result of being excited by dynamic loading [42].

Finally, the influence of boundary condition on the deflection and axial stress of the sector plate is displayed in Figs. 24 and 25.

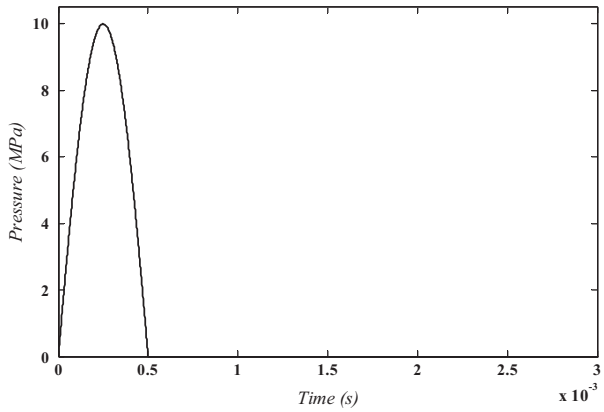

Fig. 17. Variation of lateral pressure (p_z) with time.

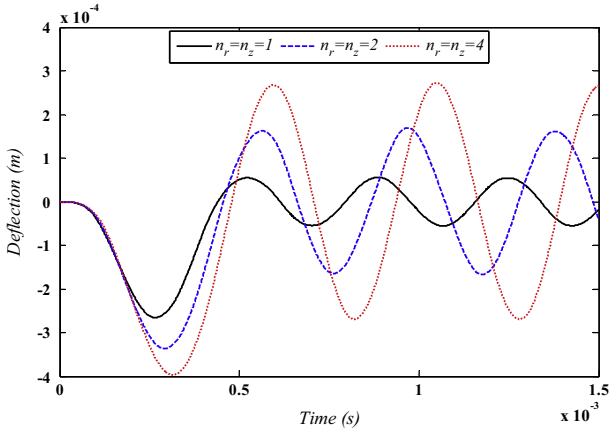

Fig. 18. Time history of the central deflection for different power law exponents.

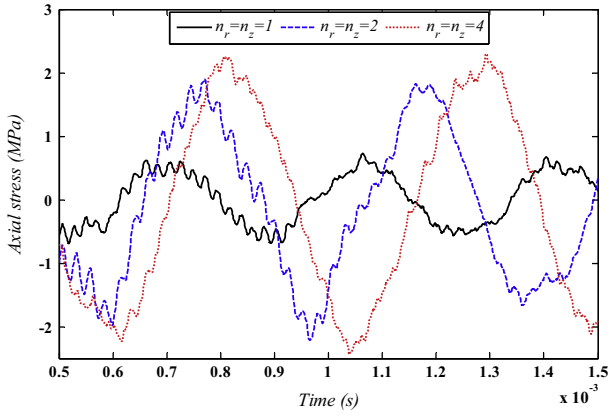

Fig. 19. Time history of the axial stress at the center point for different power law exponents.

In this case, the thickness to radius ratio is assumed to be $h/b = 0.1$ and power law exponents are $n_r = 2$ and $n_z = 3$. Similar to static behavior, the effect of boundary condition on deflection is more noticeable than stresses.

The achieved results denote that employing a graded element has several benefits compared to conventional elements, especially in the dynamic and wave propagation analyses. In the conventional FE methods, continuous material properties gradation is approximated by homogenous elements so that adjacent elements may

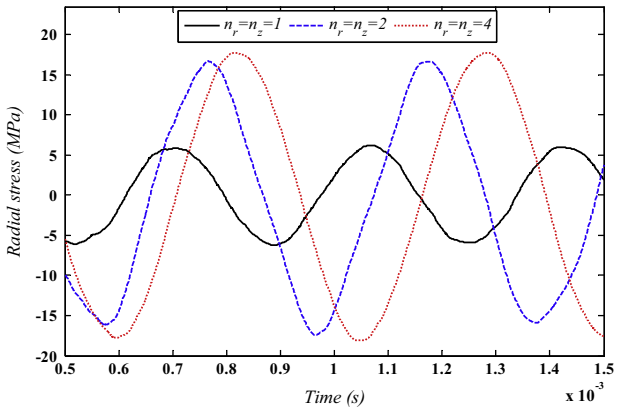

Fig. 20. Time history of the radial stress at the center point for different power law exponents.

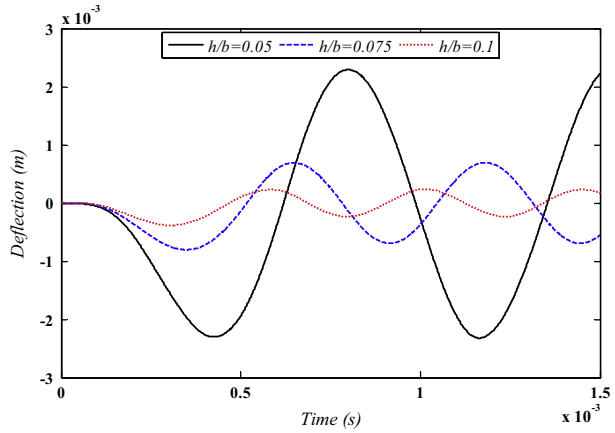

Fig. 21. Time history of the central deflection for different thickness to radius ratios.

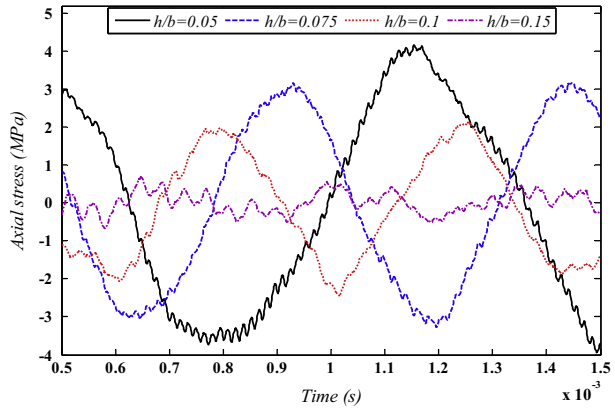

Fig. 22. Time history of the axial stress at the center point for different thickness to radius ratios.

have quite different isotropic material properties. Thus, jumps in the material properties are observed at the boundaries of these homogenous elements and this phenomenon causes artificial wave reflections which has in turn cumulative effects on magnitude and stress wave propagation velocity. Therefore, by using the graded elements wherein the material properties vary continuously in the element scale, the desired accuracy may be obtained without refining the mesh size.

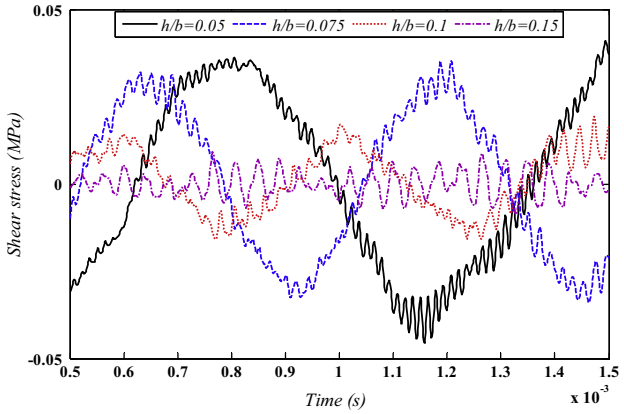

Fig. 23. Time history of the shear stress ($\sigma_{r\theta}$) at the center point for different thickness to radius ratios.

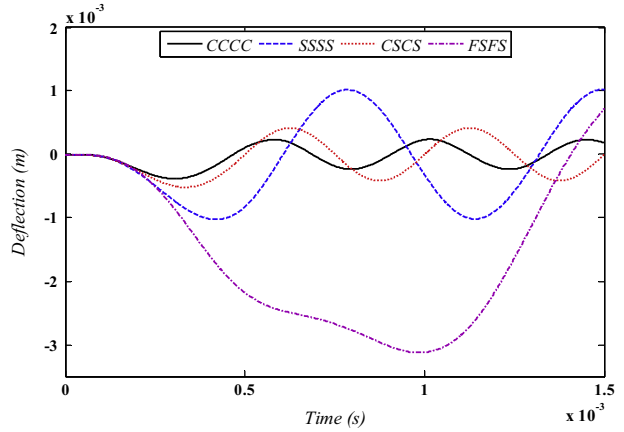

Fig. 24. Time history of the central deflection for different boundary conditions.

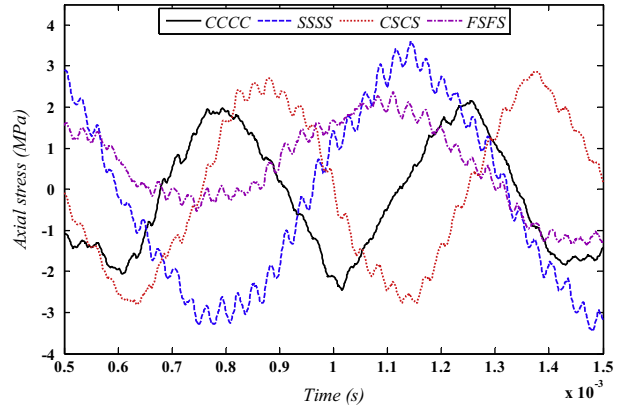

Fig. 25. Time history of the axial stress at the center point for different boundary conditions.

4. Conclusion

The main purpose of the present research was to investigate the 3D static and dynamic behavior of 2D-FG thick sector plates. The governing equations were based on the 3D theory of elasticity. In order to solve the equations in space and time domains, the 3D GFEM based on Hamilton's principle and Rayleigh–Ritz energy formulation was applied. The proposed method was verified by three examples. The comparisons between the results showed that the

present method had a good agreement with the existing results. Different types of displacement and stresses in three directions were presented for various values of power law exponents and thickness to radius ratios of the thick sector plate. Newmark's numerical integration method was employed to derive time histories of the displacement and stress components. Results denote that the static and dynamic responses of the structure can be controlled and optimized by variation of the material properties in two directions. In other words, by selecting proper heterogeneity parameters, the distribution of the deflection and stress components can be modified to satisfy the desirable requirements. Furthermore, results confirm that using 2D-FGMs leads to more flexible designs compared to 1D-FGMs.

Appendix A

The components of $\boldsymbol{\Phi}$ are:

$$\Phi_i = \frac{1}{\Omega}\boldsymbol{\Gamma}\cdot\boldsymbol{X} \tag{A1}$$

where Ω is the volume of each element that is:

$$\Omega = \begin{vmatrix} 1 & \xi_1 & \eta_1 & \zeta_1 & \xi_1\eta_1 & \xi_1\zeta_1 & \eta_1\zeta_1 & \xi_1\eta_1\zeta_1 \\ 1 & \xi_2 & \eta_2 & \zeta_2 & \xi_2\eta_2 & \xi_2\zeta_2 & \eta_2\zeta_2 & \xi_2\eta_2\zeta_2 \\ 1 & \xi_3 & \eta_3 & \zeta_3 & \xi_3\eta_3 & \xi_3\zeta_3 & \eta_3\zeta_3 & \xi_3\eta_3\zeta_3 \\ 1 & \xi_4 & \eta_4 & \zeta_4 & \xi_4\eta_4 & \xi_4\zeta_4 & \eta_4\zeta_4 & \xi_4\eta_4\zeta_4 \\ 1 & \xi_5 & \eta_5 & \zeta_5 & \xi_5\eta_5 & \xi_5\zeta_5 & \eta_5\zeta_5 & \xi_5\eta_5\zeta_5 \\ 1 & \xi_6 & \eta_6 & \zeta_6 & \xi_6\eta_6 & \xi_6\zeta_6 & \eta_6\zeta_6 & \xi_6\eta_6\zeta_6 \\ 1 & \xi_7 & \eta_7 & \zeta_7 & \xi_7\eta_7 & \xi_7\zeta_7 & \eta_7\zeta_7 & \xi_7\eta_7\zeta_7 \\ 1 & \xi_8 & \eta_8 & \zeta_8 & \xi_8\eta_8 & \xi_8\zeta_8 & \eta_8\zeta_8 & \xi_8\eta_8\zeta_8 \end{vmatrix} \tag{A2}$$

and

$$\Gamma_{ij} = (-1)^{i+j}|\Upsilon_{ij}| \tag{A3}$$

$$\boldsymbol{X} = \{1, \xi, \eta, \zeta, \xi\eta, \xi\zeta, \eta\zeta, \xi\eta\zeta\}^T \tag{A4}$$

in which

$$\xi = r\cos\theta,\ \ \eta = r\sin\theta,\ \ \zeta = z \tag{A5}$$

$$\xi_i = r_i\cos\theta_i,\ \ \eta_i = r_i\sin\theta_i,\ \ \zeta_i = z_i \tag{A6}$$

where r_i, θ_i and z_i are nodal coordinates and Υ_{ij} is obtained from eliminating the ith row and jth column of Ω.

References

[1] Miyamoto Y, Kaysser WA, Rabin BH. Functionally graded materials: design, processing and applications. Kluwer, Dordrecht; 1999.
[2] Koizumi M. The concept of FGM. Ceram Trans, Functionally Gradient Mater 1993;34:3–10.
[3] Kobayashi H, Turvey GJ. Elastic small deflection analysis of annular sector Mindlin plates. Int J Mech Sci 1994;36(9):811–27.
[4] Salehi M, Turvey GJ. Elastic large deflection response of annular sector plates, a comparison of DR finite-difference, finite element and other numerical solutions. Comput Struct 1991;40(5):1267–91.
[5] Salehi M, Shahidi A. Large deflection analysis of elastic Mindlin sector plates. Comput Struct 1994;52(5):987–98.
[6] Aghdam MM, Mohammadi M, Erfanian V. Bending analysis of thin annular sector plates using extended Kantorovich method. Thin-Walled Struct 2007;45:983–90.
[7] Aghdam MM, Shahmansouri N, Mohammadi M. Extended Kantorovich method for static analysis of moderately thick functionally graded sector plates. Math Comput Simul 2012;86:118–30.
[8] Aghdam MM, Mohammadi M. Bending analysis of thick orthotropic sector plates with various loading and boundary conditions. Compos Struct 2009;88:212–8.
[9] Mousavi SM, Tahani M. Analytical solution for bending of moderately thick radially functionally graded sector plates with general boundary conditions using multi-term extended Kantorovich method. Composites B 2012;43:1405–16.
[10] Tahani M, Mousavi SM. Analytical solution for bending problem of moderately thick composite annular sector plates with general boundary conditions and loadings using multi-term extended Kantorovich method. Arch Appl Mech 2013;83:969–85.
[11] Jomehzadeh E, Saidi AR, Atashipour SR. An analytical approach for stress analysis of functionally graded annular sector plates. Mater Des 2009;30:3679–85.
[12] Malekzadeh P, Golbahar Haghighi MR, Gholami M. Dynamic response of thick laminated annular sector plates subjected to moving load. Compos Struct 2010;92:155–63.
[13] Sharma A, Nath Y, Sharda HB. Nonlinear transient analysis of moderately thick laminated composite sector plates. Commun Nonlinear Sci Numer Simul 2007;12:1101–14.
[14] Alibeigloo A. Three-dimensional thermo-elasticity solution of sandwich cylindrical panel with functionally graded core. Compos Struct 2014;107:458–68.
[15] Shariyat M, Asemi K. Three-dimensional non-linear elasticity-based 3D cubic B-spline finite element shear buckling analysis of rectangular orthotropic FGM plates surrounded by elastic foundations. Compos B 2014;56:934–47.
[16] Jabbari M, Shahryari E, Haghighat H, Eslami MR. An analytical solution for steady state three dimensional thermoelasticity of functionally graded circular plates due to axisymmetric loads. Eur J Mech A/Solids 2014;47:124–42.
[17] Asemi K, Salehi M, Akhlaghi M. Three dimensional biaxial buckling analysis of functionally graded annular sector plate fully or partially supported on Winkler elastic foundation. Aerosp Sci Technol. doi: 10.1016/j.ast.2014.04.011.
[18] Asemi K, Salehi M, Akhlaghi M. Post-buckling analysis of FGM annular sector plates based on three dimensional elasticity graded finite elements. Int J Non-Linear Mech 2014;67:164–77.
[19] Hosseini-Hashemi Sh, Salehipour H, Atashipour SR, Sburlati R. On the exact in-plane and out-of-plane free vibration analysis of thick functionally graded rectangular plates: explicit 3-D elasticity solutions. Composites B 2013;46:108–15.
[20] Attallah KMZ, Yu M, Ye JQ. Three-dimensional state space spline finite strip analysis of angle-plied laminates. Composites B 2014;66:25–35.
[21] Cheng ZQ, Batra RC. Three-dimensional thermoelastic deformations of a functionally graded elliptic plate. Composites B 2000;31:97–106.
[22] Na KS, Kim JH. Three-dimensional thermal buckling analysis of functionally graded materials. Composites B 2004;35:429–37.
[23] Malekzadeh P, Afsari A, Zahedinejad P, Bahadori R. Three-dimensional layerwise-finite element free vibration analysis of thick laminated annular plates on elastic foundation. Appl Math Model 2010;34:776–90.
[24] Setoodeh AR, Tahani M, Selahi E. Transient dynamic and free vibration analysis of functionally graded truncated conical shells with non-uniform thickness subjected to mechanical shock loading. Composites B 2012;43:2161–71.
[25] Andakhshideh A, Tahani M. Interlaminar stresses in general thick rectangular laminated plates under in-plane loads. Composites B 2013;47:58–69.
[26] Maturi DA, Ferreira AJM, Zenkour AM, Mashat DS. Analysis of sandwich plates with a new layerwise formulation. Composites B 2014;56:484–9.
[27] Setoodeh AR, Karami G. A solution for the vibration and buckling of composite laminates with elastically restrained edges. Compos Struct 2003;60:245–53.
[28] Roque CMC, Ferreira AJM, Jorge RMN. Modelling of composite and sandwich plates by a trigonometric layerwise deformation theory and radial basis functions. Composites B 2005;36:559–72.
[29] Shariyat M, Alipour MM. Semi-analytical consistent zigzag-elasticity formulations with implicit layerwise shear correction factors for dynamic stress analysis of sandwich circular plates with FGM layers. Composites B 2013;49:43–64.
[30] Alipour MM, Shariyat M. Analytical stress analysis of annular FGM sandwich plates with non-uniform shear and normal tractions, employing a zigzag-elasticity plate theory. Aerosp Sci Technol 2014;32:235–59.
[31] Nemat-Alla M. Reduction of thermal stresses by composition optimization of two-dimensional functionally graded materials. Acta Mech 2009;208:147–61.
[32] Asemi K, Salehi M, Akhlaghi M. Elastic solution of a two-dimensional functionally graded thick truncated cone with finite length under hydrostatic combined loads. Acta Mech 2011;217(1–2):119–34.
[33] Zafarmand H, Hassani B. Analysis of two-dimensional functionally graded rotating disks with variable thickness. Acta Mech 2014;225:453–64.
[34] Kim JH, Paulino GH. Isoparametric graded finite elements for nonhomogeneous isotropic and orthotropic materials. J Appl Mech 2002;69:502–14.
[35] Ashrafi H, Asemi K, Shariyat M, Salehi M. Two-dimensional modeling of heterogeneous structures using graded finite element and boundary element methods. Meccanica 2012;48:663–80.
[36] Zafarmand H, Kadkhodayan M. Three-dimensional static analysis of thick functionally graded plates using graded finite element method. Proc Inst Mech Eng, C 2014;228:1275–85.
[37] Boresi AP, Chong KP, Lee JD. Elasticity in engineering mechanics. 3rd ed. Hoboken, New Jersey: John Wiley & Sons Inc; 2011.
[38] Zienkiewicz OC, Taylor RL. The finite element method for solid and structural mechanics. 6th ed. Oxford: Elsevier Butterworth-Heinemann; 2005.
[39] Kashtalyan M. Three-dimensional elasticity solution for bending of functionally graded rectangular plates. Eur J Mech A/Solids 2004;23:853–64.
[40] Sahraee S. Bending analysis of functionally graded sectorial plates using Levinson plate theory. Compos Struct 2009;88:548–57.
[41] Abaqus. Version 6.12-1, Dassault Systems Inc.; 2012.
[42] Xue H, Hu HP. Nonlinear characteristics of a circular plate piezoelectric harvester with relatively large deflection near resonance. IEEE Trans Ultrason Ferroelectr Freq Control 2008;55(9):2092–6.